

Space-Time Ground-Level PM_{2.5} Distribution at the Yangtze River Delta: A Comparison of Kriging, LUR, and Combined BME-LUR Techniques

L. Xiao¹, G. Christakos^{1,2*}, J. Y. He¹, and Y. C. Lang¹

¹ Ocean College, Zhejiang University, Zhoushan, 316000, China

² Department of Geography, San Diego State University, San Diego, CA, 92182-4493, USA

Received 1 April 2016; revised 7 February 2018; accepted 28 March 2018; published online 1 July 2020

ABSTRACT. Ambient air PM_{2.5} is one of the major pollutants linked to respiratory and lung diseases in the Yangtze River Delta (YRD), which is China's leading economic region and one of the top economic regions worldwide. The main objectives of this work is to compare the accuracy of some widely-used techniques to characterize and predict the space-time distribution of ground-level PM_{2.5} in the YRD, and to propose a synthesis of techniques that can yield better results than previous techniques. First, a land-use regression (LUR) model is implemented using the relevant data bases (such as air quality, aerosol optical depth, AOD, Modern-Era Retrospective analysis for Research and Applications, MERRA, meteorological monitoring, road networks information, longitude, latitude, elevation and land-use data). Then, the synthesis of the LUR and the Bayesian maximum entropy (BME) techniques is proposed and implemented, for the first time, in the study of PM_{2.5} concentrations over the YRD region. It was found that the combined (integrated) BME-LUR technique generated PM_{2.5} concentration estimates showing a 28.34% improvement in accuracy (R^2 indicator) compared to the standard LUR technique, and a 12.53% improvement compared to the mainstream geostatistical Kriging technique.

Keywords: the Yangtze River, PM_{2.5}, the Bayesian Maximum Entropy, the land-use regression, aerosol optical depth

1. Introduction

Particulate matter PM_{2.5} (particles less than 2.5 μm in diameter) is one of the major pollutants causing adverse health effects, including respiratory lung diseases. PM_{2.5} concentrations grow rapidly worldwide seriously affecting people's daily-life, especially in economically developed and urbanized countries (Kunzli et al., 2000; Duki et al., 2003; Bogaert et al., 2009). During the last 30 years, China has experienced a fast-growing economy and industrial development. As a result, several studies have shown that haze pollution has gradually become a severe environmental problem in China since the 1990s (Che et al., 2007; Zhao et al., 2011; Ma et al., 2016b). Yet, it was not until the end of 2012 that a nationwide PM_{2.5} monitoring network was established. Concerning human exposure assessment in China, we lack long-term and large-scale PM_{2.5} concentration datasets, which are not available before 2013.

The study of pollutant health effects depends on the accurate exposure estimation at unmonitored locations (e.g., residential places) and time periods (e.g., of high human activity). Accurate space-time estimation is a key prerequisite of health studies, like the minimization of human exposure misclassifi-

cation. In order to improve the accuracy of PM_{2.5} concentration estimation across space-time, different quantitative techniques of space-time analysis of the pollutant of interest, estimation and mapping have been developed (Ryan et al., 2008; Beckerman et al., 2013; Hu et al., 2013; Adam-Poupart, 2013; Hu et al., 2014a; Reyes and Serra, 2014; Liu et al., 2016; Christakos et al., 2017; He et al., 2018a). Specifically, land-use regression (LUR) (Briggs et al., 1997; Gilliland et al., 2005) is a technique that predicts pollutant concentrations at unmonitored (unsampled) locations as a function of georeferenced variables (topography, traffic, and other geographic variables). LUR consists of five major components: dependent variable (pollutant concentration), monitoring network, land use maps, buffers (i.e., radii of defined distances for the geographic variables of interest), and a set of independent variables (Liu et al., 2016). The dependent variable is the pollutant of interest and measurements come from a monitoring network. Kriging (Olea, 1999) is another regression-type interpolation technique that estimates pollutant values at unmonitored locations as a linear combination of weighted observations at monitoring stations. Bayesian maximum entropy (BME) (Christakos, 1990) is a knowledge-synthesis theory of space-time modeling and estimation. Unlike the LUR and Kriging techniques, BME is a non-linear estimator that can consider non-Gaussian distributions, in general, and, in addition to hard data it can integrate various kinds of soft data and core knowledge in the spatio-temporal domain (e.g., Christakos and Vyas, 1998; Bell, 2006; Bogaert et al., 2009; He et al., 2018b).

* Corresponding author. Tel.: +619-594-8285; Fax: +619-594-8285

E-mail address: gchrista@sdsu.edu (G. Christakos).

The main objectives of this work are (i) to compare the accuracy of certain techniques that are widely-used to predict the ground-level $PM_{2.5}$ distribution in the case of the Yangtze river delta (YRD) during the period January 1, 2015 ~ May 31, 2016, and (ii) to propose a synthesis of techniques that can yield better results. Geographically, the YRD is located near the 30° North latitude on the eastern coast of mainland China. It is an alluvial plain before the Yangtze River flows into the East China Sea. The YRD lies within the subtropical monsoon climate zone, with high temperatures and heavy and hot rains during the summer. The YRD includes the Shanghai, Jiangsu and Zhejiang provinces. It is China's largest economic zone, the central government's most comprehensive economic center in China, and one of the world's most advanced manufacturing bases. Before 2013 Beijing-Tianjin-Hebei was a region of highly $PM_{2.5}$ -related disease-incidence, and since 2013 the YRD has become another severe haze polluted area with high $PM_{2.5}$ -re-lated incidence. Hence, improving air quality is arguably a major challenge in this region (Hu et al., 2016). In view of these considerations, the present work is a comparative study that uses: (a) an LUR technique based on the available data (air quality, aerosol optical depth, AOD, modern era retrospective analysis, MERRA, meteorological monitoring data, road networks information, longitude, latitude, land-use data, and digital elevation modeling, DEM); (b) two forms of combined BME-LUR techniques (BME-LUR^(a) and BME-LUR^(b)) incorporating $PM_{2.5}$ monitoring station data and soft data produced by land-use regression; and, finally, (c) a mainstream Kriging technique based on $PM_{2.5}$ monitoring station data. These four techniques are implemented in the YRD study region, assuming a 3-km AOD data to estimate high-resolution $PM_{2.5}$ concentrations in this region. Then the relative performance of these techniques is assessed quantitatively, an efficient BME-LUR synthesis is proposed, and some conclusions are drawn that could be useful to the practitioners and researches using these techniques.

2. Material and Method

2.1. Study Area

As noticed above, the YRD region is located in the south-east coastal zone of China (Figure 1). The mainstream delineation of the YRD region includes the metropolitan Shanghai area and the economically developed and urbanized southern part of Jiangsu province and the northern part of the Zhejiang province. An expanded delineation of the YRD region (Fang et al., 2011) includes the Shanghai, Jiangsu, Zhejiang and Anhui provinces, with a population of about 160 million (NBS, 2012). The present study focuses on the Shanghai, Jiangsu and Zhejiang areas. The locations of the $PM_{2.5}$ monitoring sites in the YRD region are also shown in Figure 1.

2.2. Data

2.2.1. $PM_{2.5}$ Measurements

The 24-h averaged $PM_{2.5}$ concentrations at nationally-referenced monitors in the YRD study area during the period Jan-

uary 1, 2015 to May 31, 2016 were downloaded from the China Environmental Monitoring Center (CEMC, <http://106.37.208.233:20035/>). The observed $PM_{2.5}$ concentrations, which serve as the dependent variable of the estimation techniques and are modeled as a spatiotemporal random field (Christakos, 2017), include 157 $PM_{2.5}$ monitoring sites with a total of 40,848 observations in the YRD study area, and, also, 65 $PM_{2.5}$ monitoring sites that were evenly distributed in the neighboring provinces and around the monitoring sites to avoid any edge-effects. According to CNAAQs (Chinese National Ambient Air Quality Standards), those stations were omitted in which observations were available for less than 15 days within a month. Daily data were used to calculate the average $PM_{2.5}$ concentration at each site, and the average of the four seasons was obtained by using Python 2.7 (<https://www.python.org/>).

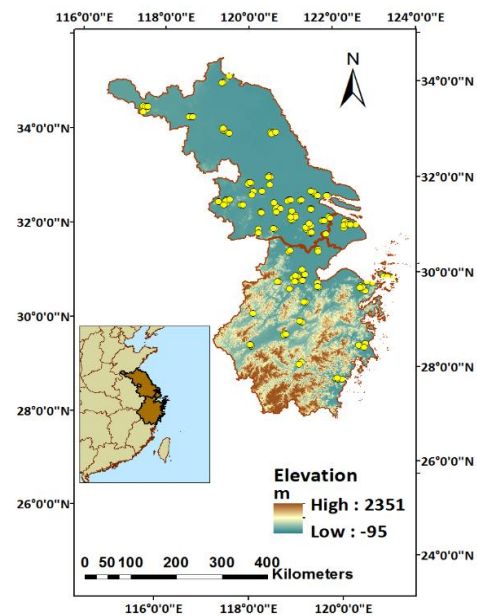


Figure 1. The yellow dots represent 157 $PM_{2.5}$ monitoring sites in the YRD region.

2.2.2. AOD Data

The aerosol optical depth (AOD) data were obtained from the newly released MODIS collection of 6 AOD products (<http://ladsweb.nascom.nasa.gov/>) with 3-km spatial resolution. The 3-km AOD (MYD04_3k, MOD04_3k) is retrieved with the help of the same dark-target algorithm, although its accuracy is slightly lower over land. MODIS is an instrument aboard the Terra and Aqua satellites operated by the National Aeronautics and Space Administration (NASA) (Remer et al., 2005). The basic principle of MODIS aerosol data was first proposed by Kaufman et al. (1997). Specifically, during the study period (January 1, 2015 to May 31, 2016) the 10:30 AM Terra and 1:30 PM Aqua were used to synthesize the Chinese regional daily AOD products. The data processing steps were as follows: (a) a geometric correction of the data was applied, and the 550 nm wavelength aerosol optical thickness data was selected after geometric correction; (b) daily data of 550 nm

wavelength aerosol optical thickness were mosaicked after the geometric correction was embedded to synthesize the daily product, and the average value of the overlapping area in the mosaic image was selected; and (c) MODIS Terra and MODIS Aqua aerosol data were synthesized in order to obtain the maximum usable range.

2.2.3. Meteorological Fields

The daily planetary boundary layer height (PBLH) and wind speed (m/s) data were obtained from the Modern-Era Retrospective analysis for Research and Applications (MERRA) product (https://gmao.gsfc.nasa.gov/pubs/office_notes/). MERRA is based on the Goddard Earth Observing System (GEOS-5) general circulation model and allows a native spatial resolution of 0.5° latitude \times 0.65° longitude (Pfeifroth et al., 2013). The data were divided into 1-h and 6-h products, which were subsequently synthesized into a daily product, with the resulting data processing steps being as follows: (i) daily documents were read according to the 24-h synthesis of the 1-h products; (ii) for precipitation data we use their sum, and for PBLH data we consider their average; (iii) 6-h product documentation is processed in the same way; and (iv) the above synthesized daily products was the output of data processing. Data were also collected daily from meteorological monitoring stations, including precipitation (m), temperature (K), relative humidity (%), and air pressure (Pa) from the China Meteorological Data Sharing Service System (<http://cdc.cma.gov.cn>).

2.2.4. Land Use Information

Many previous studies have showed that land-use information could affect the relationship between $PM_{2.5}$ concentrations and satellite AOD (Kloog et al., 2012; Ma et al., 2014; Lee et al., 2016). For land-use information, 500-m resolution surface classification data were downloaded from MODIS (Friedl et al., 2010), and we measured the total area of urban and forest cover within 200m, 500 m, 1 km, 2 km, 3 km, 4 km, 5 km, and 8 km buffers around the $PM_{2.5}$ stations, and the area was expressed in m^3 . Yet, these different buffers were not significant and they did not enter into the final model (because the p -value was > 0.05). This work also used the nearest distance to coast (in km) calculated for each monitoring site based on the coastline of the YRD region. Latitude and longitude were also considered in the model (Adam-Poupart et al., 2014; Liu et al., 2016).

2.2.5. Road Network Data

Road length data were extracted from the OpenStreetMap (<http://www.openstreetmap.org>) in which major roads, primary and secondary highways, and railways from all road layers were retained. We measured the total length (km) of such roads within 200m, 500 m, 1 km, 2 km, 3 km, 4 km, 5 km, and 8 km buffers around the $PM_{2.5}$ stations.

2.2.6. Elevation Data

The 30-m resolution digital elevation data were download-

ed from the Shuttle Radar Topography Mission (SRTM, <http://srtm.csi.cgiar.org/SELECTION/inputCoord.asp>).

2.2.7. Data Integration

For data integration purposes, and based on data pre-processing and extraction, this paper first interpolated all the meteorological data at a 3-km scale using inverse distance weighted (IDW) interpolation tools (ArcGIS 10.3) to match the AOD grid size. Then, we created a grid with a 3-km spatial resolution that included a total number of 34,453 grid cells based on interpolated meteorological data. All data were integrated into records adequate for LUR fitting, validation and mapping purposes. The data collections were re-projected to the Asia Lambert Conformal Conic coordinate system. The observed $PM_{2.5}$ concentrations from multiple in-situ stations were averaged at the corresponding grid cell. AOD and meteorological fields were assigned to each grid using the nearest neighbor method. The area of land-use cover for urban types was calculated from the land-use data in the buffers. The road length was summed up in the same buffers of land-use data. And the elevations were subsequently averaged at each grid cell.

2.3. Analysis Methods

2.3.1. Model Developments—The LUR Model

Based on the observations available at the monitoring sites, we developed a stepwise linear multiple regression (LUR) mixed-effects model to predict $PM_{2.5}$ concentrations using the SPSS software version 19.0. Being a stepwise linear regression using environmental data as independent variables, the LUR model predicts $PM_{2.5}$ seasonally averaged concentration given a group of variables. The $PM_{2.5}$ seasonally averaged concentration can be expressed using the equation:

$$\mathbf{X}_p = \beta_0 + \sum_{i=1}^k \beta_i \mathbf{Y}_{i,p} + \varepsilon_p \quad (1)$$

where \mathbf{X}_p denotes seasonally averaged $PM_{2.5}$ concentrations (recall that averaged $PM_{2.5}$ concentrations during different seasons were calculated using meteorologically daily data), β_0 is the equation intercept, the $\mathbf{Y}_{i,p}$ ($i = 1, \dots, k$) are the independent variables for the seasonal $PM_{2.5}$ concentrations at the space-time location p , ε_p is an error term, and β_i ($i = 1, \dots, k$) are the coefficients of each independent variable. In view of LUR's stepwise linear regression structure, initially a model with 36 variables was considered, and then the implementation of SPSS automatically provided the best model with 7 variables. The values of the variance inflation factors (VIFs), which are a measure of model collinearity, were calculated for the LUR model. If a variable within a model has a VIF value greater than 10, that particular variable is considered to be collinear with the remaining variables in a model. The VIF for the j^{th} variable in a model of m variables is:

$$VIF = 1/(1 - r_j^2) \quad (2)$$

where r_j is the correlation coefficient from regressing the j^{th}

variable on the remaining $m - 1$ variables. Note that each model produces m VIF values. If any one of them is greater than 10, the model is said to have collinearity and is not considered as the final optimum LUR model. The incorporation of site-specific variables into the model detected small area variations, and the VIFs values of the final optimum LUR model were all less than 10.

2.3.2. The BME Technique

BME is a spatiotemporal modeling and prediction theory with very general features, e.g., it is non-linear and non-Gaussian, and it incorporates space-time information from many different sources, core and site-specific (Christakos, 1990, 2000). Its implementation is made possible in terms of various software libraries, like the one used here, namely, the Spatiotemporal Epistemic Knowledge Synthesis Graphical User Interface software library (SEKS-GUI-v0.8) (Yu et al., 2007). The basic set of BME equations of space-time $PM_{2.5}$ estimation used in the present YDR study are (Christakos, 2000, 2010):

$$\int dG(\mathbf{g} - \bar{\mathbf{g}})e^{\mu \cdot \mathbf{g}} = 0 \quad (3a)$$

$$\int dS e^{\mu \cdot \mathbf{g}} - Af(\mathbf{X}_p) = 0 \quad (3b)$$

where \mathbf{g} is a vector of functions expressing mathematically the available core knowledge base G , including spatiotemporal covariance models, exposure laws, and scientific theories, including the LUR model; $\bar{\mathbf{g}}$ denotes the mean value of \mathbf{g} ; S represents the available site-specific (i.e., the YRD in this case) knowledge base about the pollutant as described earlier, including AOD, MERRA, meteorological monitoring data, road networks information, land-use data, and DEM; μ is a vector of coefficients representing the relative importance of each \mathbf{g} -function ($\mu \cdot \mathbf{g}$ denotes the inner product of the vectors \mathbf{g} and μ , which are both functions of space-time); and A is a normalization parameter. Equations (3a and b) can be solved with respect to the $PM_{2.5}$ probability law $f(\mathbf{X}_p)$ at all disease mapping points of interest (i.e., space-time points at which BC predictions are sought). Software libraries have been developed dealing with the solution of Equations (3a and b) in real world conditions, including BMElib, QuantumBME, and StarBME (e.g., Yu et al., 2007). More technical details and physical interpretations of the basic BME equations above can be found in the relevant literature.

BME is able to combine core or general knowledge (theoretical models, physical laws, and scientific relationships) about the attribute of interest with site-specific knowledge (hard data and soft data in the form of uncertain measurements, probabilistic assessments and auxiliary information). In this work, the core knowledge includes a mean trend function and a theoretical covariance model, and site-specific knowledge comes from seasonally averaged $PM_{2.5}$ concentration. Site-specific knowledge can either be considered hard or soft. Hard data includes site-specific measurements with little or no uncertain-

ty associated with them. Soft data includes site-specific knowledge characterized by various levels of uncertainty in the form of uncertain observations, auxiliary information, and probabilistic assessments (probability distribution functions, PDF, Gaussian, interval, uniform, triangle etc.). This allows BME to rigorously integrate any non-Gaussian soft data, such as soft data with a truncated Gaussian distribution (Reyes and Serre, 2014). Also, it has been proven in theory that Kriging is a special case of BME under limiting conditions linear estimation, Gaussian distribution and hard only site-specific data (Christakos, 2000).

2.3.3. BME-LUR and Kriging Techniques

We applied the BME-LUR and Kriging techniques to estimate space-time $PM_{2.5}$ concentrations in an economically developed southeast coastal area. The hard data that served as input to the Kriging technique included the measured $PM_{2.5}$ concentration values at monitoring stations for all eligible station-days during the period January 1, 2015 to May 31, 2016 (all predictions are about seasonally-averaged data). On the other hand, two hard data forms were used by the BME-LUR techniques:

- (i) the measured $PM_{2.5}$ concentration dataset (for BME-LUR^(a)), and
- (ii) the residual $PM_{2.5}$ seasonally-averaged concentrations provided by LUR based on the $PM_{2.5}$ monitoring stations (for BME-LUR^(b)).

Otherwise said, in the BME-LUR setup, the LUR model is the input to the BME technique. The soft data generated by the LUR model and used in the BME-LUR^(a) technique consisted of $PM_{2.5}$ estimates at each location and an associated confidence interval (each location was the center of the $50 \text{ km} \times 50 \text{ km}$ grid cell). For BME-LUR^(b) and Kriging we used only hard data (i.e., no soft data estimates from the LUR model were considered in these two techniques).

2.3.4. 10-Fold Cross-Validation between Spatiotemporal Estimation and Ground Observations

The coefficient of determination (R^2), mean error (ME), mean absolute prediction error (MAE), and root mean squared prediction error (RMSE) were the accuracy indicators calculated between the estimates generated by each spatiotemporal estimation technique (LUR, BME-LUR^(a), BME-LUR^(b), and Kriging) vs. ground observations in order to assess the performance of each technique. The estimates generated by each technique used the same dataset, and, thus, they did not experience potential over-fitting (i.e., the situation where the estimation technique performs well in the context of the dataset used for model fitting, but poorly at locations and during days outside this dataset).

Specifically, we used a sample-based, 10-fold cross validation (CV) technique (Lee et al., 2011) to test the potential over-fitting of the spatiotemporal estimation techniques. In terms of the k -fold cross-validation classification error estimator (k -cv) technique, the data set is divided into k folds (in this case, $k = 10$), a classifier is learned using $k - 1$ folds, and an

error value is calculated by testing the classifier in the remaining fold. Finally, the k -cv estimation of the error is the average value of the errors committed in each fold. Thus, the k -cv error estimator depends on two factors: the training set and the partition into folds (Rodriguez et al. 2010). Previous BME-LUR studies mainly used the leave-one-out validation method (Adam-Poupart et al., 2014; Reyes and Serre, 2014). In terms of the sample-based 10-fold CV method, all samples in the dataset were randomly divided into 10 subsets with equal numbers of samples. One subset served as the testing base, and the remaining nine subsets were used to test the values generated by the spatial estimation techniques during each validation round. Since the sample-based, 10-fold CV method has been more widely used in previous PM_{2.5}-AOD modeling studies than the site-based CV technique (Chang et al., 2014), in this study we selected the sample-based 10-fold CV method.

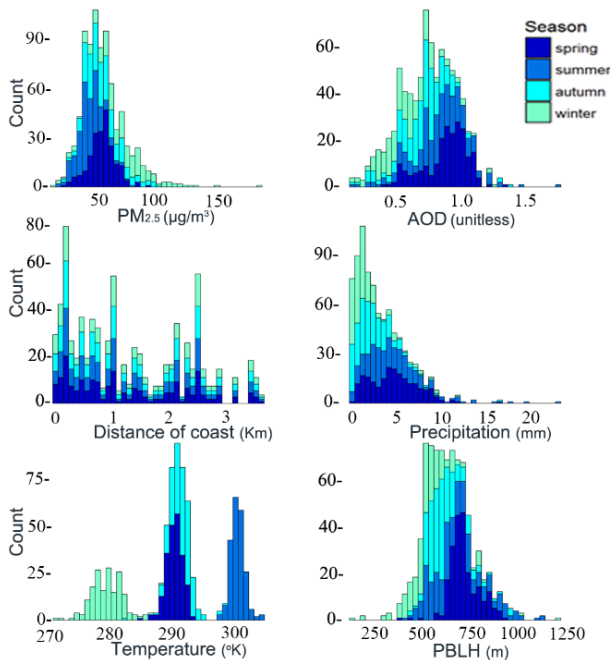


Figure 2. Histogram and summary statistics of the LUR model variables for the seasonally monitored datasets ($N = 830$ estimated points).

3. Results

3.1. Descriptive Statistics

The seasonal histograms and summary statistics of the LUR variables are plotted in Figure 2 and Table 1. Various simulations of models with 36 variables were initially generated, and then the model was selected with 7 independent variables. In particular, the yearly average PM_{2.5} concentration, AOD, temperature, planetary PBLH, precipitation, distance to coast, longitude and latitude were calculated: 54.49 µg/m³, 0.76, 2910 K, 637.5 m, 3.34 mm, 140.72 km, 119.4° and 31.51°, respectively. Table 2 summarizes the main features of the LUR model with the highest value of $R^2 = 0.440$ generated with seasonally-

averaged PM_{2.5} concentrations using the 7 independent variables above. The three time scales (i.e., daily-, monthly- and yearly-averaged scales) of the LUR models gave the indicator R^2 values 0.170, 0.366, and 0.339, respectively. All independent variables were statistically significant at the $\alpha = 0.05$ level for the LUR techniques. Concerning the effect of each variable: the AOD, temperature, longitude, and distance to coast were found to be the main predictors; the AOD and latitude had a positive association with PM_{2.5}; and the temperature, PBLH, longitude, precipitation and distance to coast showed negative associations with PM_{2.5} concentrations. These findings are consistent with the fixed effects shown in previous implementations of the LUR technique in China (Adam-Poupart et al., 2014; Li et al., 2015; Liu et al., 2016; Ma et al., 2016a, b; Meng et al., 2016). Note that the LUR technique produced 7 distinct VIF values (corresponding to the 7 independent variables). Since all of them were < 10 , the technique was considered collinearity-free, and the 7 variables were selected into the final optimum LUR technique.

Table 1. Descriptive Statistics of Modeling Dataset

Variable	Min	Median	Mean	Max
PM _{2.5} (µg/m ³)	11.5	51.42	54.49	183.0
Temperature (K)	272.0	291.1	291.1	304.8
Latitude (°N)	26.69	31.42	31.51	35.42
AOD (unitless)	0.147	0.758	0.756	1.736
PBLH (m)	131.1	629.1	637.5	1196.1
Longitude (°E)	116.8	119.6	119.4	122.3
Precipitation (mm)	0.0	258.8	333.6	2302.8
Distance of Coast (km)	0.07	103.2	130.4	363.2

Table 2. Summary of the LUR Model Variables

Seasonal model	Regression coefficients	Significant	VIF
Intercept	914.384	.000	
Temperature (K)	-1.247	.000	1.356
Latitude (°N)	1.296	.001	2.232
AOD (unitless)	19.918	.000	1.709
PBLH (m)	-.024	.000	1.467
Longitude (°E)	-4.445	.000	9.903
Precipitation (mm)	-.603	.001	1.242
Distance of Coast (km)	-3.664	.006	7.969
Adjusted R ²	0.440		

3.2. Covariance Model Fitting

Concerning the empirical space-time covariances presented in Figure 3 we notice that the covariances of the combined BME-LUR techniques showed a sharp drop after the space origin, whereas they displayed a very slow decline along the time axis. This dual behavior indicates a short correlation range in space and a long correlation range in time. By comparison, the covariance of the Kriging technique showed the slowest decrease across space implying a longer spatial correlation than the models of the other techniques, whereas the covariance of

the BME-LUR^(a) technique experienced the slower decrease in time implying a longer temporal correlation space (given that there are only four seasons, the temporal correlation of adjacent seasons is stronger).

In light of these features of the empirical covariances, the following theoretical covariance models were fitted to the empirical ones:

(1) BME-LUR^(a)

$$c_{r_1}(h, \tau) = c_1 e^{-3\left(\frac{h^2 + \tau}{a_{s_1} a_{t_1}}\right)} + c_2 e^{-3\frac{h}{a_{s_2}}\left(1 - \frac{3\tau}{2a_{t_2}} + \frac{\tau^3}{2a_{t_2}^3}\right)} \quad (4)$$

(2) BME-LUR^(b)

$$c_{r_2}(h, \tau) = c_3 e^{-3\frac{h^2}{a_{s_3}^2}\left(1 - \frac{3\tau}{2a_{t_3}} + \frac{\tau^3}{2a_{t_3}^3}\right)} + c_4 e^{-3\left(\frac{h}{a_{s_4}} + \frac{\tau}{a_{t_4}}\right)} \quad (5)$$

(3) Kriging

$$c_{r_3}(h, \tau) = c_5 \left(1 - \frac{3h}{2a_{s_5}} + \frac{h^3}{2a_{s_5}^3}\right) \left(1 - \frac{3\tau}{2a_{t_5}} + \frac{\tau^3}{2a_{t_5}^3}\right) + c_6 \left(1 - \frac{3h}{2a_{s_6}} + \frac{h^3}{2a_{s_6}^3}\right) \left(1 - \frac{3\tau}{2a_{t_6}} + \frac{\tau^3}{2a_{t_6}^3}\right) + c_7 e^{-3\frac{h}{a_{s_7}}\left(1 - \frac{3\tau}{2a_{t_7}} + \frac{\tau^3}{2a_{t_7}^3}\right)} \quad (6)$$

where $[c_1, c_2, c_3, c_4, c_5, c_6, c_7] = [0.6, 0.4, 0.54, 0.46, 0.32, 0.45, 0.23]$, $[a_{s_1}, a_{s_2}, a_{s_3}, a_{s_4}, a_{s_5}, a_{s_6}, a_{s_7}] = [0.15, 0.3, 0.1, 0.25, 0.1, 0.2, 2]$ in degrees, and $[a_{t_1}, a_{t_2}, a_{t_3}, a_{t_4}, a_{t_5}, a_{t_6}, a_{t_7}] = [6.3, 3, 3, 3, 3, 3.2, 4]$ in quarters. Using the above covariance models, we obtained BME estimates that are representative of the actual PM_{2.5} distribution and spread.

3.3. Cross Validation

Figure 4 and Table 3 show the cross-validation (CV) results of the four space-time estimation techniques. The BME-LUR^(b) was the most accurate among them ($R^2 = 0.548$) with the lowest RMSE (12.382 $\mu\text{g}/\text{m}^3$). The BME-LUR^(a) ($R^2 = 0.483$, RMSE = 13.946382 $\mu\text{g}/\text{m}^3$) and the Kriging techniques ($R^2 = 0.487$, RMSE = 13.2382 $\mu\text{g}/\text{m}^3$) performed better and with greater precision than the LUR technique ($R^2 = 0.427$, RMSE = 13.779382 $\mu\text{g}/\text{m}^3$). Compared to the LUR, BME-LUR^(a) and Kriging techniques, the BME-LUR^(b) technique also performed best at the seasonal scale. This is a key feature of BME-LUR^(b), i.e., it is an effective integration of BME and LUR that combines multi-sourced data and predicts accurately the air pollution distributions in a composite space-time domain.

3.4. Spatial Distributions of PM_{2.5} Predictions

Figure 5 presents ground-level PM_{2.5} measurements and the seasonal mean PM_{2.5} predictions using the four different

space-time techniques. First, we notice that the spatial patterns of the LUR and BME-LUR^(b) predictions of the PM_{2.5} concentrations are very similar, and they are both characterized by some missing data. This is due to the fact that the MODIS 3-km AOD data were retrieved by the Dark Target (DT) algorithm, and DT-AOD cannot be retrieved over bright surfaces, thus causing a considerable number of AOD missing values in bright urban or water areas. Most of the PM_{2.5} monitoring sites are clustered in urban areas in China, which may impact the performance of a space-time estimation technique (Ma et al., 2016b). Although BME-LUR^(a) and Kriging predictions do not involve any missing values, the BME-LUR^(b) technique provides more spatial details due its incorporation of soft data. For example, without the inclusion of the LUR model, the small “hot spots” in Wenzhou, Ruian, and the northeast part of Cangnan during the winter would have been missed. Also, unlike the BME-LUR^(b) technique, the other three techniques tend to greatly underestimate PM_{2.5} at low concentrations.

Table 3. 10-Fold Cross-validation Results of the Space-time Estimation Techniques for the 2015 ~ 2016 Seasonal PM_{2.5} Averages

Method	R ²	RMSE	MAE	ME
LUR	0.427	13.779	10.028	-0.040
BME-LUR ^(b)	0.548	12.382	8.623	0.184
BME-LUR ^(a)	0.483	13.946	9.428	0.305
Kriging	0.487	13.200	9.281	0.223

* $k = 222$ monitoring stations, $N = 830$ estimated points

Spatially, the PM_{2.5} concentrations were high in the northern part of the study area, especially in the Jiangsu province. The spatial gradient of PM_{2.5} concentration showed a little change during the summer. During the winter and autumn, however, the spatial gradient of PM_{2.5} concentration changed significantly, and the overall trend was high in the north and low in the south, which is consistent with previous YRD studies (Zou, 2016; Zhang et al, 2017). Temporally, the PM_{2.5} concentration in the YRD region showed an obvious seasonal variation, the average PM_{2.5} concentration during winter (which reached 80.39 $\mu\text{g}/\text{m}^3$) was significantly higher than that during the other three seasons.

4. Discussions

In this work, for the first time integrated BME-LUR techniques are applied in the study of space-time PM_{2.5} concentrations in the YRD region (China). The latest MODIS 3-km AOD dataset was used to estimate ground-level PM_{2.5} concentrations in the southeast coastal zone of China. Benefiting from wide spatial and temporal coverage, satellite data have been proven to be a powerful supplementary tool to estimate PM_{2.5} concentrations in regions without sufficient ground-level measurements (Hu et al., 2014b; Li et al., 2015; Ma et al., 2016a; You et al., 2016; Zou, 2016).

Overall, our findings suggest that the PM_{2.5} estimation accuracy can be improved considerably by integrating the

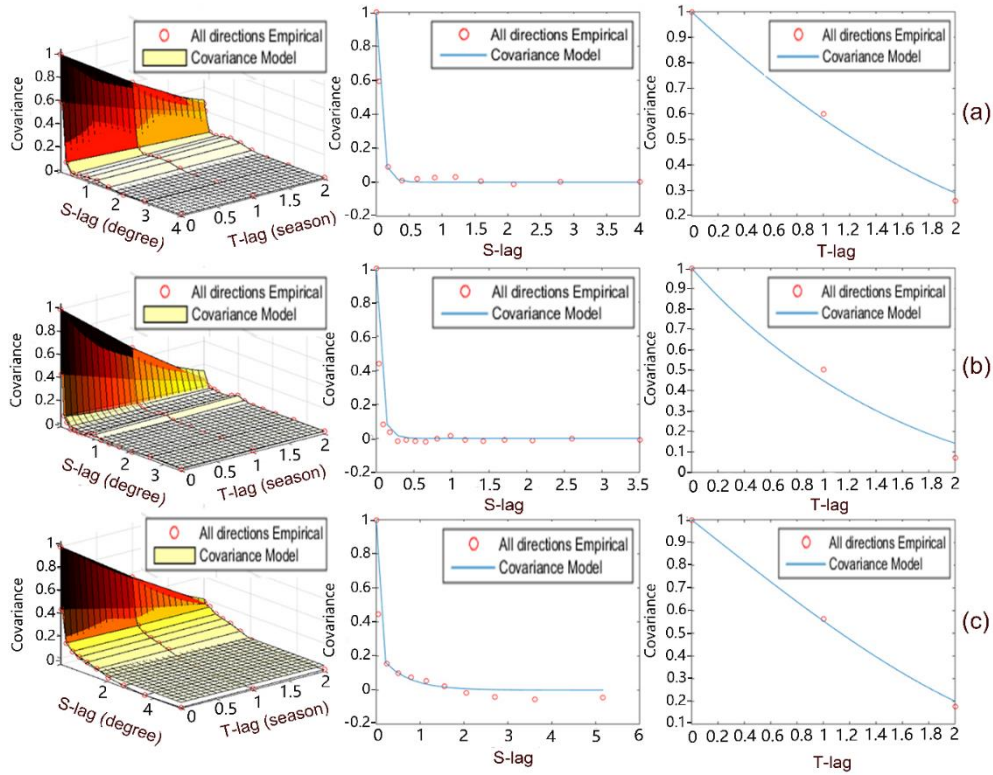


Figure 3. Spatiotemporal empirical covariances and fitted theoretical models used by the BME techniques: (a) BME-LUR^(a), (b) BME-LUR^(b), and (c) Kriging.

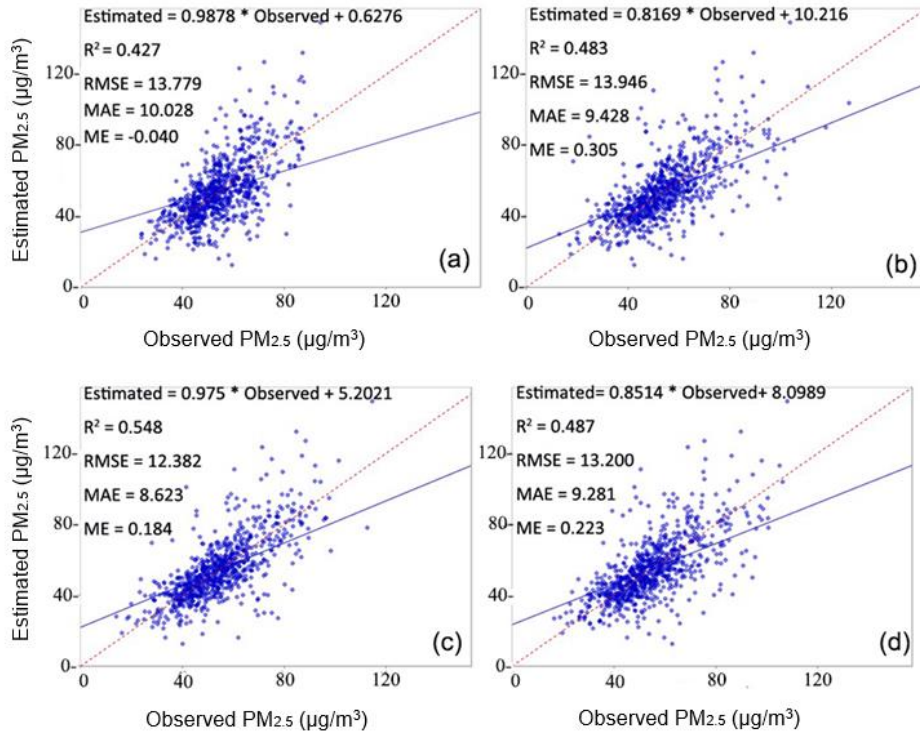


Figure 4. CV results for the four models ($N = 830$, $t = 4$): (a) LUR, (b) BME-LUR^(a), (c) BME-LUR^(b), and (d) Kriging. Dashed lines are the 1:1 lines, for reference. Solid lines are the regression lines.

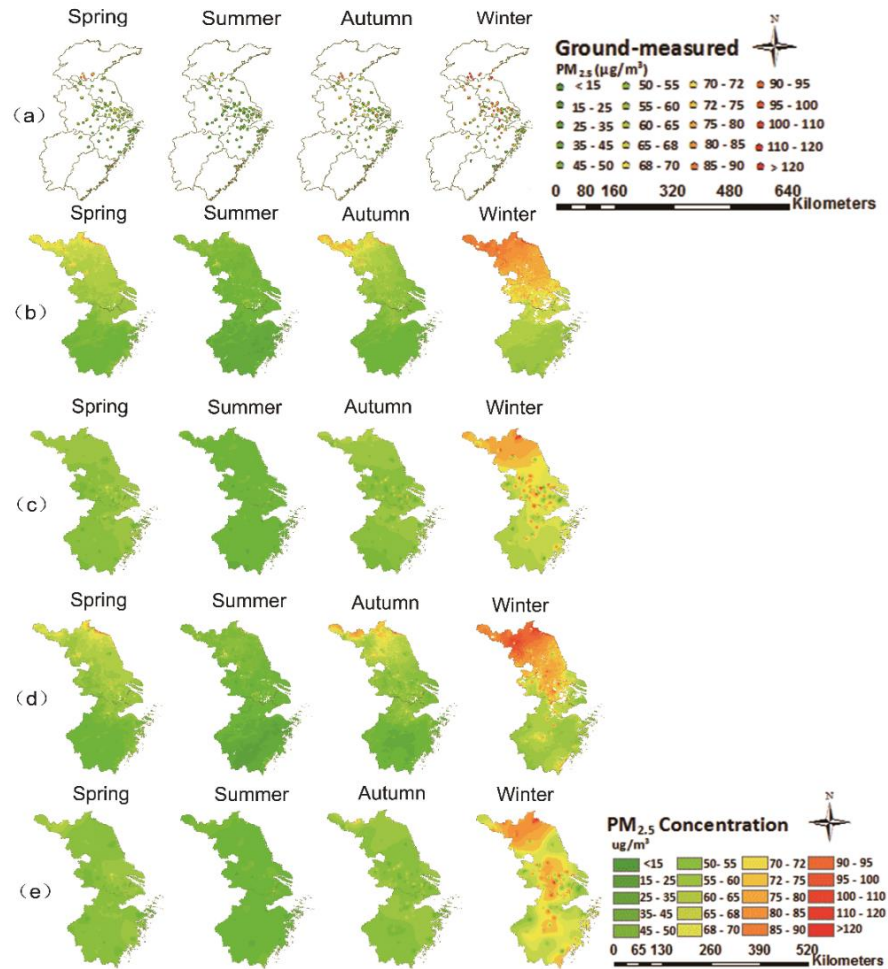


Figure 5. (a) Ground measurements and spatial distributions of seasonal PM_{2.5} predictions for the four space-time estimation techniques: (b) LUR, (c) BME-LUR^(a), (d) BME-LUR^(b), and (e) Kriging

BME technique in the analysis compared to other commonly used techniques. In particular, the BME-LUR^(b) technique had the best performance in terms of 10-fold cross-validations with accuracy indicator values, $R^2 = 0.548$, RMSE = 12.382, and MAE = 8.623. The proposed BME-LUR^(b) technique showed a 28.3% improvement in R^2 , a 14% reduction in MAE and a 1.4 g/m³ reduction in RMSE compared to the existing techniques.

It should be noticed that Adam-Poupart et al. (2014) also compared the LUR technique (PM_{2.5} estimation accuracy indicators: $R^2 = 0.466$, RMSE = 8.747) vs. the BME technique ($R^2 = 0.653$, RMSE = 7.057), and it was found that BME was more accurate with respect to both accuracy indicators (R^2 and RMSE). Reyes and Serre (2014) improved PM_{2.5} estimation across the USA from 1999 to 2009 by combining the LUR model (which accounted for on road mobile and stationary source emissions) with the BME technique ($R^2 = 0.78$, RMSE = 1.12, MAE = 0.63). Their LUR-BME technique ($R^2 = 0.53$) improved R^2 by 47.17% compared to the LUR model. Yu et al. (2011) used a combined LUR-BME model with road and land use data to predict seasonal PM_{2.5}/PM₁₀ concentrations in the Taipei area (Taiwan) during 2005 ~ 2007. We notice that the

BME-LUR technique of Reyes and Serre (2014) covered a larger study area and more types of environment variables than Yu et al. (2011). Although most of earlier studies did not report any accuracy indicator values, the mean of their pollutant estimation errors were higher than those of our present study. In particular, the mean error (ME) for BME-LUR (Yu et al., 2011) was 2.156 vs. the ME of BME-LUR (present study) that was found to be 0.184. All of the above show that the integration of BME can improve considerably the LUR model.

Furthermore, in the present study we collected and processed more data on environmental factors than previous studies, such as 3-km AOD, PBLH and temperature, we explored the relationship between them and PM_{2.5} pollution, and we incorporated a LUR model into the BME estimation technique. The calculated accuracy indicators of the combined BME-LUR techniques showed a considerable improvement compared to the LUR technique.

Future work could consider (i) adding more data sources, such as 1-km AOD data (Wang et al., 2010; Lin et al., 2015; Wu et al., 2016), (ii) interpolating more accurate meteorological data by means of spatial interpolation software for climatic data

(ANUSPLIN) instead of the simple IDW technique, (iii) considering different pollution sources and visualizing exposure estimates in ArcEngine 10 in order to properly assess the long-term effects of PM_{2.5} exposure on human health and facilitate better prevention and control of PM_{2.5} in the YRD region.

Acknowledgements. The authors acknowledge with appreciation the valuable suggestions provided by Dr. Chutian Zhang of the College of Natural Resources and Environment, Northwest A&F University (China) and Dr. Xufeng Fei of the Ocean College, Zhejiang University (China). The work was supported by grants by the National Natural Science Foundation of China (Grant No. 529105-N11701ZJ) and the National Science Foundation of China (Grant No. 41671399).

References

- Adam-Poupart, A., Brand, A., Fournier, M., Jerrett, M., and Smargiassi, A. (2014). Spatiotemporal modeling of ozone levels in Quebec (Canada): A comparison of kriging, land-use regression (LUR), and combined bayesian maximum entropy-LUR approaches. *Environ. Health Perspect.*, 122, 970-976. <https://doi.org/10.1289/ehp.1306566>
- Beckerman, B.S., Jerrett, M., Serre, M., Martin, R.V., Lee, S.J., Donkelaar, A.V., Ross, Z., Su, J., and Burnett, R.T. (2013). A Hybrid Approach to Estimating National Scale Spatiotemporal Variability of PM_{2.5} in the Contiguous United States. *Environ. Sci. Technol.*, 47:7233-7241. <https://doi.org/10.1021/es400039u>
- Bell, M.L. (2006). The use of ambient air quality modeling to estimate individual and population exposure for human health research: A case study of ozone in the Northern Georgia Region of the United States. *Environ. Int.*, 32, 586-593. <https://doi.org/10.1016/j.envint.2006.01.005>
- BMElib. Bayesian Maximum Entropy Library for Space/Time Geostatistics, Version 2.0b for MATLAB. https://mserre.sph.unc.edu/BMElab_web/?ga=2.98340764.2082685715.1567002294-1159773137.1548255484.
- Bogaert, P., Christakos, G., Jerrett, M., and Yu, H.L. (2009). Spatiotemporal modelling of ozone distribution in the State of California. *Atmos. Environ.*, 43, 2471-2480. <https://doi.org/10.1016/j.atmosenv.2009.01.049>
- Briggs D.J., Collins, S., Elliott, P., Fischer, P., Kingham, S., Lebre, E., Pyl, K., Van Reeuwijk, H., Smallbone, K., and Van der Veen, A. (1997). Mapping urban air pollution using GIS: a regression-based approach. *Int. J. Geogr. Inform. Sci.*, 11, 699-718. <https://doi.org/10.1080/136588197242158>
- Chang, H.H., Hu, X.F., and Liu, Y. (2014). Calibrating MODIS aerosol optical depth for predicting daily PM_{2.5} concentrations via statistical downscaling. *J. Exposure Anal. Environ. Epidemiol.*, 24, 398-404. <https://doi.org/10.1038/jes.2013.90>
- Che, H.Z., Zhang, X.Y., Li, Y., Zhou, Z.J., and Qu, J.J. (2007). Horizontal visibility trends in China 1981-2005. *Geophys. Res. Lett.*, 34. <https://doi.org/10.1029/2007GL031450>
- NBS (National Bureau of Statistics). (2012) *China Statistical Yearbook*. China Statistics Press, Beijing.
- Christakos G. (1990). A Bayesian Maximum-Entropy view to the spatial estimation problem. *Math. Geol.*, 22, 763-777. <https://doi.org/10.1007/BF00890661>
- Christakos G (2000). *Modern Spatiotemporal Geostatistics*. Oxford University Press, New York.
- Christakos, G. and Vyas, V.M. (1998). A composite space/time approach to studying ozone distribution over Eastern United States. *Atmos. Environ.*, 32, 2845-2857. [https://doi.org/10.1016/S1352-2310\(98\)00407-5](https://doi.org/10.1016/S1352-2310(98)00407-5)
- Christakos G. (2010) *Integrative Problem-Solving in a Time of Decadence*. Springer, New York, NY. <https://doi.org/10.1007/978-90-481-9890-0>
- Christakos, G. (2017). *Spatiotemporal Random Fields: Theory and Applications*. Elsevier, Amsterdam, Netherlands. <https://doi.org/10.1016/B978-0-12-803012-7.00002-7>
- Christakos, G., Yang, Y., Wu, J.P., Zhang, C.T., Mei, Y., and He, J.Y., (2017). Improved space-time mapping of PM_{2.5} distribution using a domain transformation method. *Ecol. Indic.*, 85, 1273-1279. <https://doi.org/10.1016/j.ecolind.2017.08.007>
- Duki, M.I.Z., Sudarmadi, S., Suzuki, S., Kawada, T., and Tri-Tugaswati, A. (2003). Effect of air pollution on respiratory health in Indonesia and its economic cost. *Arch. Environ. Health*, 58, 135-143. <https://doi.org/10.3200/AEOH.58.3.135-143>
- Fang, C., Yao, S., and Liu, S. (2011). *Report on Development of City Clusters in China*. Pages ISBN 978-977-903-030643-030642. Science Press.
- Friedl, M.A., Sulla-Menasse, D., Tan, B., Schneider, A., Ramankutty, N., Sibley, A., and Huang, X. (2010). MODIS Collection 5 global land cover: Algorithm refinements and characterization of new datasets. *Remote Sens. Environ.*, 114, 168-182. <https://doi.org/10.1016/j.rse.2009.08.016>
- He, J.Y. and Kolovos, A. (2018a). Bayesian maximum entropy approach and its applications: A review. *Stochastic Environ. Res. Risk Assess.*, 32, 859-877. <https://doi.org/10.1007/s00477-017-1419-7>
- He, J.Y. and Christakos, G. (2018b). Space-time PM_{2.5} mapping in the severe haze region of Jing-Jin-Ji (China) using a synthetic approach. *Environ. Pollut.*, 240, 319-329. <https://doi.org/10.1016/j.envpol.2018.04.092>
- Hu, X.F., Waller, L.A., Al-Hamdan, M.Z., Crosson, W.L., Estes, M.G., Estes, S.M., Quattrochi, D.A., Sarnat, J.A., and Liu, Y. (2013). Estimating ground-level PM_{2.5} concentrations in the southeastern US using geographically weighted regression. *Environ. Res.*, 121, 1-10. <https://doi.org/10.1016/j.envres.2012.11.003>
- Hu, X.F., Waller, L.A., Lyapustin, A., Wang, Y.J., Al-Hamdan, M.Z., Crosson, W.L., Estes, M.G., Estes, S.M., Quattrochi, D.A., Puttaswamy, S.J., and Liu, Y. (2014a). Estimating ground-level PM_{2.5} concentrations in the Southeastern United States using MAIAC AOD retrievals and a two-stage model. *Remote Sens. Environ.*, 140, 220-232. <https://doi.org/10.1016/j.rse.2013.08.032>
- Hu, J.L., Wang, Y.G., Ying, Q., and Zhang, H.L. (2014b). Spatial and temporal variability of PM_{2.5} and PM₁₀ over the North China Plain and the Yangtze River Delta, China. *Atmos. Environ.*, 95, 598-609. <https://doi.org/10.1016/j.atmosenv.2014.07.019>
- Kaufman, Y.J., Tanre, D., Remer, L.A., Vermote, E.F., Chu, A., and Holben, B.N. (1997). Operational remote sensing of tropospheric aerosol over land from EOS moderate resolution imaging spectroradiometer. *J. Geophys. Res.-Atmos.*, 102, 17051-17067. <https://doi.org/10.1029/96JD03988>
- Kloog, I., Nordio, F., Coull, B.A., and Schwartz, J. (2012). Incorporating local land use regression and satellite aerosol optical depth in a hybrid model of spatiotemporal PM_{2.5} exposures in the Mid-Atlantic States. *Environ. Sci. Technol.*, 46, 11913-11921. <https://doi.org/10.1021/es302673e>
- Kunzli, N., Kaiser, R., Medina, S., Studnicka, M., Chanel, O., Filliger, P., Herry, M., Horak, F., Puybonnieux-Textier, V., Quenel, P., Schneider, J., Seethaler, R., Vergnaud, J.C., and Sommer, H. (2000). Public-health impact of outdoor and traffic-related air pollution: a European assessment. *Lancet.*, 356, 795-801. [https://doi.org/10.1016/S0140-6736\(00\)02653-2](https://doi.org/10.1016/S0140-6736(00)02653-2)
- Lee, H.J., Chaffield, R.B., and Strawa, A.W. (2016). Enhancing the applicability of satellite remote sensing for PM_{2.5} estimation using MODIS Deep Blue AOD and land use regression in California, United States. *Environ. Sci. Technol.*, 50, 6546-6555. <https://doi.org/10.1021/acs.est.6b01438>
- Lee, H.J., Liu, Y., Coull, B.A., Schwartz, J., and Koutrakis, P. (2011).

- A novel calibration approach of MODIS AOD data to predict PM_{2.5} concentrations. *Atmos. Chem. Phys.*, 11, 7991-8002. <https://doi.org/10.5194/acp-11-7991-2011>
- Li, R., Gong, J.H., Chen, L.F., and Wang, Z.F. (2015). Estimating ground-level PM_{2.5} using fine-resolution satellite data in the megacity of Beijing, China. *Aerosol Air Qual. Res.*, 15, 1347-1356. <https://doi.org/10.4209/aaqr.2015.01.0009>
- Lin, C.Q., Li, Y., Yuan, Z.B., Lau, A.K.H., Li, C.C., and Fung, J.C.H. (2015). Using satellite remote sensing data to estimate the high-resolution distribution of ground-level PM_{2.5}. *Remote Sens. Environ.*, 156, 117-128. <https://doi.org/10.1016/j.rse.2014.09.015>
- Liu, C., Henderson, B.H., Wang, D., Yang, X., and Peng, Z.-R. (2016). A land use regression application into assessing spatial variation of intra-urban fine particulate matter (PM_{2.5}) and nitrogen dioxide (NO₂) concentrations in City of Shanghai, China. *Sci. Total Environ.*, 565, 607-615. <https://doi.org/10.1016/j.scitotenv.2016.03.189>
- Ma, Z. W., Hu, X.F., Huang, L., Bi, J., and Liu, Y. (2014). Estimating Ground-level PM_{2.5} in China using satellite remote sensing. *Environ. Sci. Technol.*, 48, 7436-7444. <https://doi.org/10.1021/es5009399>
- Ma, Z.W., Hu, X.F., Sayer, A.M., Levy, R., Zhang, Q., Xue, Y.G., Tong, S.L., Bi, J., Huang, L., and Liu, Y. (2016a). Satellite-based spatiotemporal trends in PM_{2.5} concentrations: China, 2004-2013. *Environ. Health Perspect.*, 124, 184-192. <https://doi.org/10.1289/ehp.1409481>
- Ma, Z.W., Liu, Y., Zhao, Q.Y., Liu, M.M., Zhou, Y.C., and Bi, J. (2016b). Satellite-derived high resolution PM_{2.5} concentrations in Yangtze River Delta Region of China using improved linear mixed effects model. *Atmos. Environ.*, 133, 156-164. <https://doi.org/10.1016/j.atmosenv.2016.03.040>
- Meng, X., Fu, Q.Y., Ma, Z.W., Chen, L., Zou, B., Zhang, Y., Xue, W.B., Wang, J.N., Wang, D.F., Kan, H.D., and Liu, Y. (2016). Estimating ground-level PM₁₀ in a Chinese city by combining satellite data, meteorological information and a land use regression model. *Environ. Pollut.*, 208, 177-184. <https://doi.org/10.1016/j.envpol.2015.09.042>
- Pfeifroth, U., Mueller, R., and Ahrens, B. (2013). Evaluation of Satellite-Based and Reanalysis Precipitation Data in the Tropical Pacific. *J. Appl. Meteorol. Climatol.*, 52, 634-644. <https://doi.org/10.1175/JAMC-D-12-049.1>
- Remer, L.A., Kaufman, Y.J., Tanre, D., Mattoo, S., Chu, D.A., Martins, J.V., Li, R.R., Ichoku, C., Levy, R.C., Kleidman, R.G., Eck, T.F., Vermote, E., and Holben, B.N. (2005). The MODIS aerosol algorithm, products, and validation. *J. Atmos. Sci.*, 62, 947-973. <https://doi.org/10.1175/JAS3385.1>
- Reyes, J.M. and Serre M.L. (2014). An LUR/BME framework to estimate PM_{2.5} explained by on road mobile and stationary sources. *Environ. Sci. Technol.*, 48, 1736-1744. <https://doi.org/10.1021/es4040528>
- Rodriguez, J.D., Perez, A., and Lozano, J.A. (2010). Sensitivity Analysis of k-Fold Cross Validation in Prediction Error Estimation. *IEEE Trans. Pattern Anal. Mach. Intell.*, 32, 569-575. <https://doi.org/10.1109/TPAMI.2009.187>
- Wang, Z.F., Chen, L.F., Tao, J.H., Zhang, Y., and Su, L. (2010). Satellite-based estimation of regional particulate matter (PM) in Beijing using vertical-and-RH correcting method. *Remote Sens. Environ.*, 114, 50-63. <https://doi.org/10.1016/j.rse.2009.08.009>
- Wu, J., Yao, F., Li, W., and Si, M. (2016). VIIRS-based remote sensing estimation of ground-level PM_{2.5} concentrations in Beijing-Tianjin-Hebei: A spatiotemporal statistical model. *Remote Sens. Environ.*, 184, 316-328. <https://doi.org/10.1016/j.rse.2016.07.015>
- You, W., Zang, Z.L., Zhang, L.F., Li, Y., Pan, X.B., and Wang, W.Q. (2016). National-scale estimates of ground-level PM_{2.5} concentration in China using geographically weighted regression based on 3 km resolution MODIS AOD. *Remote Sens.*, 8. <https://doi.org/10.3390/rs8030184>
- Yu, H.L., Kolovos A., Christakos G., Chen, J.C., Warmerdam S, and Dev, B. (2007). Interactive spatiotemporal modelling of health systems: The SEKS-GUI framework. *Stoch. Environ. Res. Risk Assess.*, 21(5), 555-572. <https://doi.org/10.1007/s00477-007-0135-0>
- Yu, H.L., Wang, C.H., Liu, M.C., and Kuo, Y.M. (2011). Estimation of fine particulate matter in Taipei using landuse regression and bayesian maximum entropy methods. *Int. J. Environ. Res. Public Health.*, 8, 2153-2169. <https://doi.org/10.3390/ijerph8062153>
- Zhao, P.S., Zhang, X.L., Xu, X.F., and Zhao, X.J. (2011). Long-term visibility trends and characteristics in the region of Beijing, Tianjin, and Hebei, China. *Atmos. Res.*, 101, 711-718. <https://doi.org/10.1016/j.atmosres.2011.04.019>
- Zou, X.F. (2016). Satellite-based ground PM_{2.5} estimation using timely structure adaptive modeling. *Remote Sens. Environ.*, 152-163. <https://doi.org/10.1016/j.rse.2016.08.02>